Hindawi
Journal of Geological Research
Volume 2017, Article ID 1309053, 14 pages
https://doi.org/10.1155/2017/1309053

Research Article

Combining Resistivity and Aeromagnetic Geophysical Surveys for Groundwater Exploration in the Maghnia Plain of Algeria

Djamel Boubaya

Water and Environment Laboratory, University of Tébessa, Route de Constantine, 12000 Tébessa, Algeria

Correspondence should be addressed to Djamel Boubaya; boubaya_d@yahoo.com

Received 21 July 2016; Revised 15 November 2016; Accepted 13 December 2016; Published 18 January 2017

Academic Editor: Umberta Tinivella

The Maghnia plain in western Algeria is filled by Plio-Quaternary and Miocene sediments that rest unconformably on a basement of Jurassic rocks. Electrical sounding (VES), magnetic data, well information, and hydrogeological data have been used to explore for groundwater potential in the Maghnia plain. The interpretation of Schlumberger sounding data was first calibrated with the lithology of available nearby wells. Four geoelectrical layers were identified within the study area. They are a thin near surface topsoil layer with variable resistivities, a moderate resistive aquifer (15–30 ohm-m), a resistive aquifer (40–70 ohm-m), and a conductive clay layer (1–10 ohm-m). Near Sidi Mbarek, the geoelectric section is reduced to three layers: a topsoil layer, a conductive layer corresponding to the Miocene marls, and a deep resistive layer that correlates with the Oxfordian sandstones. The interpretation of VES data and the enhancement techniques of magnetic data enabled the identification of a number of unmapped faults that occur near recharge zones close to adjacent mountains. This study enabled us to study the extension of the known Plio-Quaternary aquifer of the Maghnia plain and to explore the possible existence of a second deep groundwater aquifer in Oxfordian sandstones.

1. Introduction

The study area (Figure 1) is located in the west of the Maghnia plain close to the Algerian-Moroccan border. The Maghnia plain is the eastward extension of the Angad plain in Morocco, with the study area above the transboundary aquifer of the Angad plain [1].

The subsurface Tertiary sedimentary infill, particularly the limit between Miocene and Plio-Quaternary under the Maghnia plain, is not well understood compared with the surface outcrop exposed in the bordering mountains. Knowledge of the subsurface structure of this area is very important for groundwater exploration because an important transboundary Plio-Quaternary aquifer occurs in a graben in the study area.

According to the United Nations Development Programme (UNDP) and the World Bank, Algeria is poor in water resources with 500 m^3 per capita per year that will decrease to only 430 m^3 by the year 2020 [2]. To address the water stress resulting from a cycle of droughts, the national strategy aims to construct new dams, further exploiting groundwater resources, and to use of nonconventional resources such as sea water desalination. However, in the remote Maghnia plain near the Algerian-Moroccan border, groundwater aquifers provide the only significant way to store water during rainfall years and make it accessible during drought years for the population in this semiarid region.

For deep aquifer systems such as the Maghnia plain, detailed knowledge of the subsurface geology cannot be obtain from surface geology mapping. Geophysical techniques in general and electrical methods in particular are the most valuable methods used for hydrogeological investigations. The resistivity method has been widely used as a reconnaissance tool in groundwater investigations because it yields a good correlation between a terrain's electrical resistivity and its geology and fluid content with numerous successful case histories [3–9].

The study area has been the subject of many hydrogeological studies. Djediai et al. [10] studied the water quality of

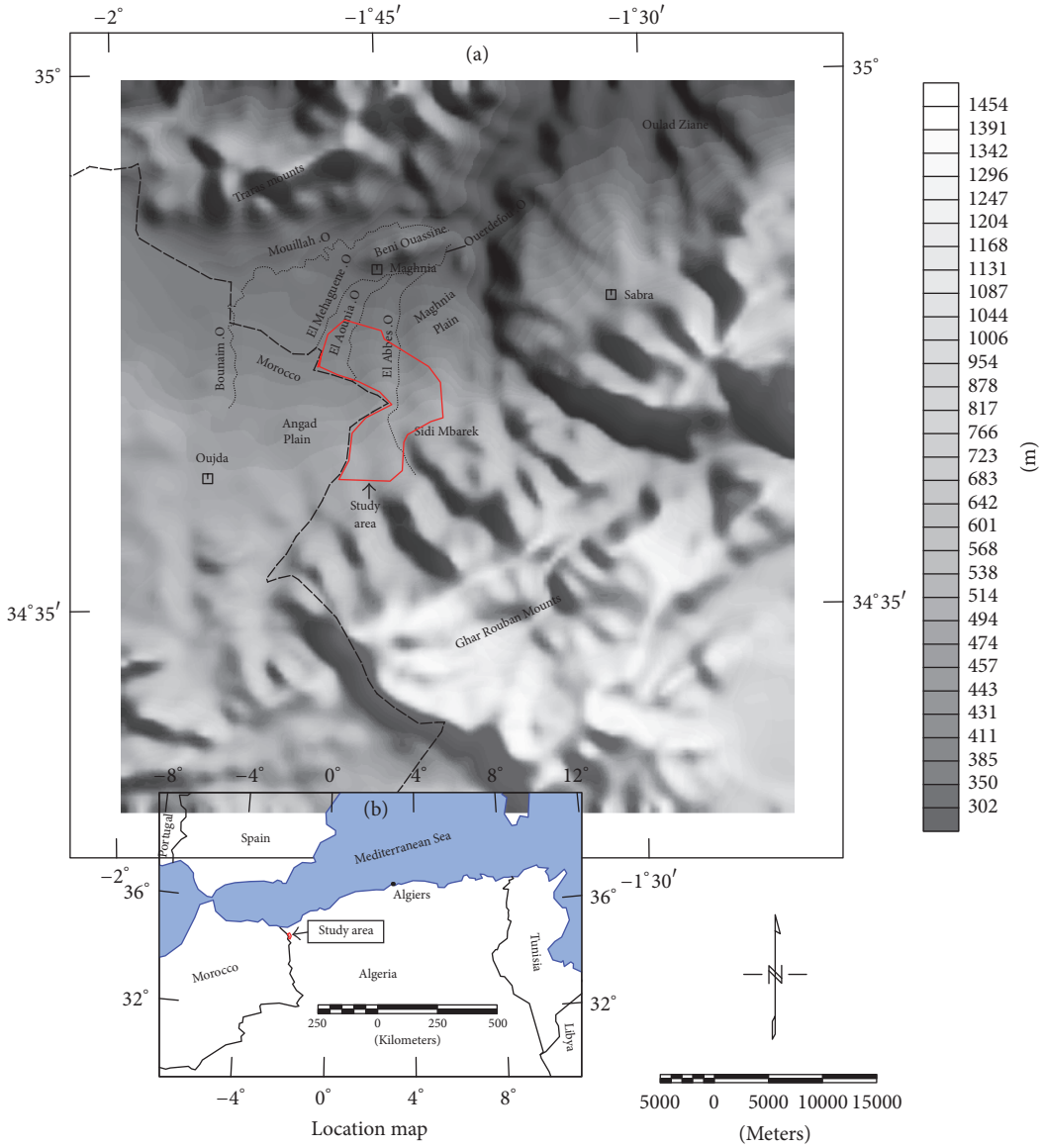

FIGURE 1: (a) Elevation map showing major features discussed in the text; (b) location map for the study area.

the Maghnia plain and concluded that the Plio-Quaternary aquifer had not yet been affected by anthropogenic pollution carried by watercourses. In the Moroccan part of the transboundary aquifer, Boughriba et al. [1] mapping in a GIS environment using the DRASTIC index assessed the vulnerability and risk of pollution of the Angad aquifer. Baba Hamed [11] studied the effect of the overexploitation of the Plio-Quaternary aquifer of the Maghnia plain and estimated using mathematical models the permeability and the water flow and its impact on the piezometric evolution of the aquifer.

The objective of the present study was (1) to explore the extension of the Plio-Quaternary aquifer to the west and (2) to investigate the groundwater possibilities of the Oxfordian sandstones under the Maghnia plain using an integration of aeromagnetic and vertical electrical sounding (VES) data. More specifically the investigation aimed to (1) study the tectonic evolution of the investigated area, (2) assess the variation of resistivity with lithology and depth, (3) outline the groundwater aquifer thickness and depth, (4) estimate the groundwater aquifer potential of the study area, and (5) find new favourable sites for new groundwater exploratory boreholes.

2. Geology

2.1. Stratigraphy. The Maghnia plain is a bowel-shaped basin oriented (ENE-WSW) that is filled by sedimentary deposits coming from the erosion of the bordering Ghar Rouban and Traras Mountains in the south and north, respectively. The Maghnia plain corresponds to a trough filled by Miocene and Quaternary sediments. The unconformably underlying Jurassic rock sequence (Figure 2) in the south of the study

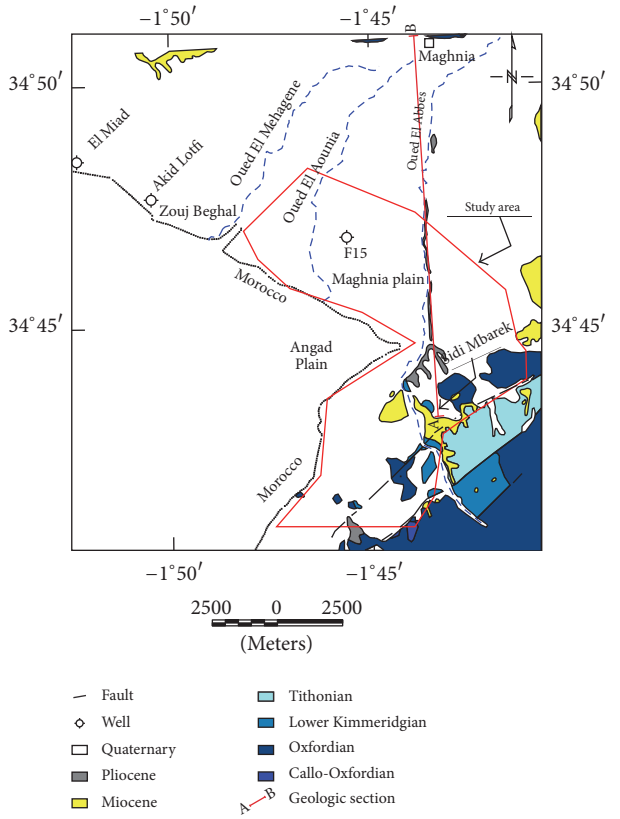

Figure 2: Geologic map of the study area (extracted from the geologic sheet of Maghnia, scale 1 : 50,000, after ORGM [12]).

Age	Lithology	Thickness	Description
Plio-Quaternary		20–120	Discontinuous mixed sediments
Miocene		50–800	Marls and sandstone
Kimmeridgian		500–600	Limestone
Oxfordian		300–400	Chalky sandstone with clay intercalations
Callo-Oxfordian		?	Monotonous set of thin beds of sandstone and marls
Bajocian-Bathonian		150–250	Layered limestones overlain by dark limestones and marls
Lias		300–400	Limestone with conglomeratic interbeds
Permo-Trias		?	Coarse sandstone with clay intercalations
Carboniferous		?	Shale
Devonian		?	Shale, and granite
Silurian		?	Shale and quartzite

Figure 3: Stratigraphy of the Maghnia plain.

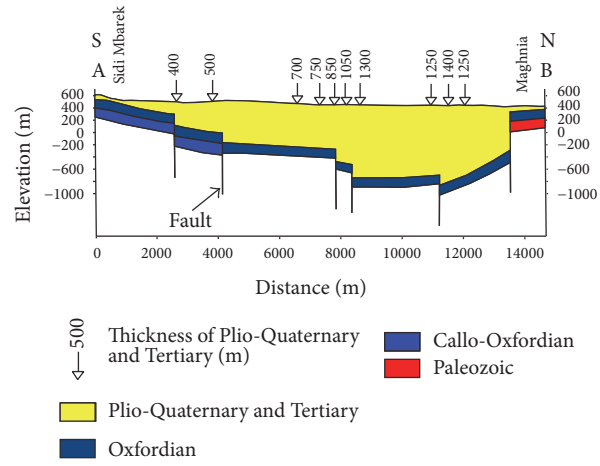

Figure 4: Geologic section showing the thickness of Plio-Quaternary and Tertiary cover.

area is dissected by normal faults generally striking northeast-southwest [12, 13].

From top to bottom, the following stratigraphic formations are present (Figure 3): (1) The Plio-Quaternary is composed of 20–120 m of discontinuous mixed sediments which overlap and crosscut with an occasional interbedded basaltic flow near Oujda in Morocco and to the north of Maghnia. (2) The Miocene is 50 to 800 m thick and outcrops near the borders of the basin as broad bands of calcareous sandstone that rest directly on Jurassic strata. When covered by alluvium, the sandstone bands are separated by thick horizons of clays or marls [14]. (3) Kimmeridgian limestones exist in the Maghnia plain only as erosional outliers but are between 500 and 600 m thick in the mountains. (4) The Oxfordian consists of a thick 300 to 400 m sequence of red chalky sandstone with clay intercalations. (5) The Callo-Oxfordian formation presents a monotonous set of thin beds of sandstone and marls that increase in percentage of clay to sandstone from west to east. (6) The Bajocian-Bathonian is made of layered limestones overlain by dark limestones and marls that varies between 150 and 250 m in thickness. (7) The Lias is mainly calcareous with conglomeratic interbeds with a total thickness of 300–400 m. (8) The Permo-Triassic consists of red coarse sandstones with clay intercalations. (9) The Paleozoic formation (Silurian, Devonian, and Carboniferous) forms the framework of the area, it corresponds roughly to a SW-NE band made up primarily of shales and quartzites that is bordered to the north and the South by Mesozoic formations.

2.2. Tectonics. The main structural features of the study area are the consequences of the Hercynian orogeny. Tectonically, the study area is part of a region of horsts and grabens that is characterized by brittle tectonics (Figure 4). The Maghnia plain itself corresponds to a graben filled with Quaternary and Tertiary sediments that is bounded to the

south (Ghar Rouban) and to the north (Traras) by horsts. The principal faults in the study area are ENE-WSW. The direction of these faults corresponds to uplifted and collapsed zones. They determine vertical displacement of 200 m with a total displacement higher than 1000 m for the whole faults. Figure 4 illustrates the thickness of Plio-Quaternary cover above Oxfordian sandstones and is compiled from well data, previous geological, and hydrogeological and geophysical studies. It shows the downdropped blocks toward the center of the plain with intervening normal faults [11–13, 15, 16].

2.3. Hydrogeology. The Maghnia plain is traversed by two separate oueds or *temporary watercourses*. They are the Mouillah oued that is an extension of the Moroccan Bounaim oued and Ouerdefou oued that is the confluence of the El Abbes, El Aounia, and El Mehaguene oueds (Figure 1(a)).

The main aquifer under the Maghnia plain is the Plio-Quaternary alluvium with the Miocene marls forming the substratum. The Plio-Quaternary fill has a variable thickness and is composed of a heterogeneous series of overlapping clays, fine or coarse sands, gravel, pebbles, and lacustrine limestone with a maximum thickness at the center of the plain [10]. Two main hydrogeological features are identified across the plain: the channel and the talus. The groundwater is divided into impermeable lenses because of vertical and horizontal lithological heterogeneity but follows a channel of an ancient river valley. The channel of the ancient river valley is oriented SW-NE with a NE slope (Figure 5). The channel does not correspond to a structural direction. It is about an old river valley cut in the Miocene marls and filled with alluvium. The talus is oriented E-W (Figure 5). At its top, it includes conglomerates containing large size slightly weathered pebbles, characteristic of a short transport and at its bottom, it is composed of clay or of sandy clay. Toward the foot of the slope, the lithology of the talus is gradually finer and passes downstream to silts without coarse material.

Apart from these two sectors (the channel and the talus), the remainder of the plain contains also coarse levels with reduced thickness and often with clay cement and hence lower porosity and permeability. With the formation of an embryonic water network, the aggradation changes and becomes mainly argillaceous.

The geological nature of the Plio-Quaternary cover suddenly changes from one place to another. The granulometry varies from clays to pebbles and the thickness of the alluvium tends to decrease near the Miocene outcrops and increases under the center of the plain. The productive alluviums are located in the uppermost 50–60 m. Below this depth, the alluviums are less permeable and may even constitute a substratum for groundwater in addition to Miocene marls. There is also a secondary channel that is oriented N-S along the El Abbes oued that will be checked by the present hydrogeophysical study. The Miocene sandstones aquifer is of a little interest because the water that infiltrates it contributes to the recharge of the Plio-Quaternary alluvium aquifer by lateral migration and so the two aquifers behave like a single one. The Kimmeridgian limestones and dolomites are aquifers when they are fractured; however, the existence of

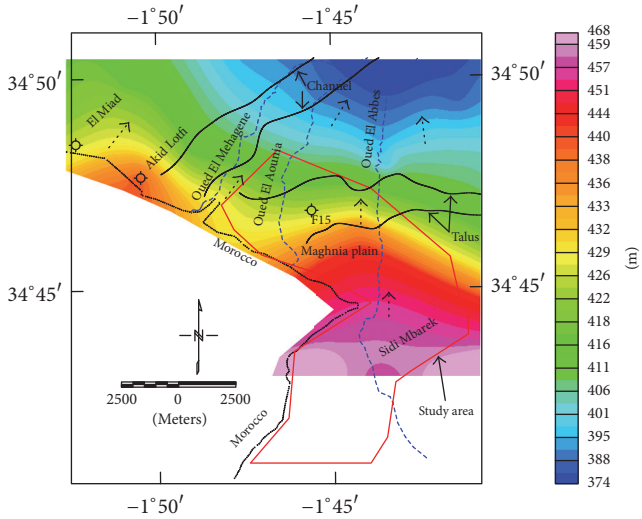

Figure 5: Iso piezometric map for the study area.

the Kimmeridgian under the Maghnia plain is uncertain. The deep borehole of Oulad Ziane (1600 m) reached the Lias without crossing the Kimmeridgian limestones and thus confirms the above assumption.

The existence of an aquifer in the Oxfordian sandstones in the southwest part of the Maghnia plain offers other possibilities for water supply. These sandstones, if they exist at depth under the Plio-Quaternary and the Miocene, could constitute a single reservoir containing considerable quantities of groundwater. This Oxfordian aquifer is exploited by farmers for self-use and small scale irrigation near Sid Mbarek in the south of the plain; however details about it are very limited. Finally, the Lias constitutes a continuous reservoir but is isolated from the other aquifers and is fed only by its own catchment area (Ghar Rouban and south of Oujda in Morocco).

Figure 5 shows a groundwater level (piezometric) map that was obtained for the study area using the data from 24 wells [11, 16]. The groundwater flow direction was determined as being toward the north and followed the course of El Mehaguene, El Aounia, and El Abbes oueds. Two different zones can be distinguished in this map: a western zone (near the Akid Lotfi well), which is characterized by a rise in the piezometric level corresponding to a strong water flow coming from Morocco, and a southern zone characterized by a higher piezometric head indicating the existence of permeable strata at shallow depths.

Meteorological data were recorded at the Office National de Météorologie (ONM, Oran). For the Maghnia station, between 1970 and 2005, the average annual temperature was 17.1°C and the average annual rainfall was 339.9 mm. The hot season extends from May to October, during which the monthly average temperatures are higher than the annual average, whereas the cold season corresponds to November–April. The maximum temperature is reached in August-July around 26°C and the minimum is reached in January around

9°C. This division of the year into two thermal seasons is not without consequence on the river flow and the hydrogeological behavior of the plain. Indeed, great monthly oscillations during the most cold months are accompanied by significant phenomena such that the brutal fall of the temperature, which involves generating rainy episodes of floods which act directly on the flow. Also, the effect of the hot season causes a rainfall deficit and an evapotranspiration from where a hydric deficit is characterized by low water levels. The dryness of the summer makes the irrigation necessary in the plain. These data highlight the continental tendency of the climate of the Maghnia plain located in a basin which is isolated from the sea influence by the mountain shielding effect of the Traras highs.

3. Geophysical Methods

3.1. Aeromagnetic Data. The aeromagnetic data used in this study were extracted from a regional-scale aeromagnetic survey of northern Algeria conducted by Aeroservice Corporation for the Société Nationale de Recherches et d'Exploitations Minières (SONAREM) from 1971 to 1974 as a part of a national mineral exploration program. The survey was conducted along NNW-SSE profiles perpendicular to the general geologic strike of the study area. The survey was flown in drape mode using Doppler-assisted navigation at an average ground clearance of 150 m and a line spacing of 2 km for traverses and 10 km for tie lines. The data were collected at a sampling interval of 46 m using a high resolution cesium magnetometer.

A whole set of processing and corrections were applied by Aeroservice to the aeromagnetic data, including magnetic levelling and the subtraction of the International Geomagnetic Reference Field (IGRF). Although Aeroservice applied standard corrections to magnetic measurements, the obtained magnetic map shows that the data always suffer from errors due to the lag effect and to microlevelling noise. The map comprises also a long wavelength regional component whose origin is not related to crustal magnetic sources but rather due to a bad estimation of the reference field IGRF-65 model.

The aeromagnetic map that we present here is processed with the greatest care; it constitutes a sufficiently precise final document for use for quantitative analysis. Details of processing applied to correct the residual errors and other noted effects in the magnetic data are published elsewhere [17, 18]. Given the average distance between flight lines of about 2 km, the grid cell size needed to make the magnetic map was chosen to be 0.5 km using minimum curvature method [19]. Thus the information contained in this map is sufficient for a regional-scale study without the appearance of undesirable noise "artifacts" often caused by a too small grid cell size. The processing and the interpretation of magnetic data were done by the software package "Oasis montaj" of Geosoft [20].

3.1.1. Reduction to the Magnetic Pole. Magnetic anomalies vary with the geographic latitude and are difficult to interpret. The reduction to the pole, method of Baranov [21], places the magnetic anomalies directly over their sources by converting their asymmetric shape to a symmetric one. The reduction to pole operator is given by the following equation [20]:

$$L(\theta) = \frac{[\sin(I) - i \cdot \cos(I) \cdot \cos(D-\theta)]^2}{[\sin^2(I_a) + \cos^2(I_a) \cdot \cos^2(D-\theta)] \cdot [\sin^2(I) + \cos^2(I) \cdot \cos^2(D-\theta)]} \quad \text{if } (|I_a| < |I|,\ I_a = I), \tag{1}$$

where I is geomagnetic inclination and I_a is inclination for magnitude correction (never less than I). The default is ±20 degrees. If $|I_a|$ is specified to be less than $|I|$ it is set to I. D is Geomagnetic declination; $i^2 = -1$.

The reduction to the pole has an amplitude component (the $\sin(I)$ term) and a phase component (the $i\cos(I)\cos(D-\theta)$ component). When reducing to the pole from equatorial latitudes, north-south features can be exaggerated due to the strong amplitude correction (the $\sin(I)$ component) that is applied when $(D-\theta)$ is $\pi/2$ (i.e., a magnetic east-west wavenumber). By specifying a higher latitude for the amplitude correction alone, this problem can be reduced or eliminated at the expense of undercorrecting the amplitudes of north-south features. An amplitude inclination of 90° causes only the phase component to be applied to the data (no amplitude correction), and a value of 0 (zero) causes phase and amplitude components to be applied over the entire range [20].

In this study, pole reduction was performed assuming induced magnetization only. An inclination of 48.8° and a declination of 354.2° were used as the parameters for reduction to the pole operator.

3.1.2. Multiscale Edge Detection. Multiscale edge detection or "worms" are vectorised points of maximum gradient derived through a process of upward continuation of potential field data [22–24]. Near surface sources induce short wavelength anomalies in the measured magnetic field, whereas deep sources induce long wavelength anomalies in the measured magnetic field. Calculating an array of upward continuation levels provides insight into the behavior of potential field gradients at different scales and depths (i.e., small upward continuations reflect gradients near surface and large upward continuations map gradients at depth). The multiscale detection process was applied to the magnetic data of part of the Maghnia plain and surrounding area with six upward levels. Prior to upward continuation, the Total Magnetic Intensity (TMI) data were reduced to pole and the horizontal gradient was subsequently determined for each level.

3.1.3. Spectral Analysis. Energy spectral analysis provides a technique for quantitative studies of large and complex aeromagnetic data sets [25]. The power spectrum of aeromagnetic total field data gives an estimate of the average depth to a group of magnetic sources. The method is based on the assumption that the magnetic effect of the basement surface can be simulated by an uncorrelated distribution of vertical prismatic blocks of varying depth, width, thickness, and magnetization.

The energy spectrum of the map in polar coordinates is

$$\langle E(r,\theta)\rangle = 4\pi^2 M^2 R_G \left\langle e^{-2hr}\right\rangle \left\langle 1-e^{-tr}\right\rangle \left\langle S^2(r,\theta)\right\rangle \left\langle R_P^2\right\rangle, \quad (2)$$

where $\langle\cdot\rangle$ indicates the expected value, $r = (u^2+v^2)^{0.5}$ is magnitude of the frequency vector, $\theta = \text{arctg}(u/v)$ is direction of the frequency vector, M is magnetic moment/unit depth, h is depth to the top of the prism, t is thickness of the prism, S is factor for the horizontal size of the prism, R_P is factor for magnetization of the prism, and R_G is factor for geomagnetic field direction.

As the parameters h and t are completely factored, their influences will simply be added in the logarithmic form of (2). The depth h enters only into the factor e^{-2hr} and its logarithm approximates a straight line whose slope is -2 h. Thus, the ensemble average depth is determined from the slope of the log-power spectrum.

3.2. Vertical Electrical Sounding (VES). In most geologic materials, the main factors governing resistivity are the concentration of ions (ionic strength) in the pore water and the amount of pore water present, since current is conveyed mostly by flowing ions in the pore water. The higher the water content and the higher the ionic strength, the lower the resistivity. Clay minerals, with their charged surfaces and associated boundary layers of attracted ions, also contribute to low resistivity [26]. Current conduction in a rock may be of electrolytic and electronic types. The resistivity of rocks and minerals varies between 10^{-6} and 10^{+14} ohm-m (a range of 10^{20}). While electronic conductivity is mainly encountered in minerals, in groundwater studies, electrolytic conductivity is most important. The conductivity is largely controlled by porosity, water content, and water quality [9].

In the VES method, the positions of the electrodes are changed with respect to a fixed point (known as the sounding point). In this way, the measured resistance values at the surface reflect the vertical distribution of resistivity values in a geological section. The VES procedure consists of passing a known amount of current (I) into the ground through two current electrodes, C_1 and C_2, and measuring the potential difference (V) developed between the potential electrodes P_1 and P_2. The spacing between the current electrodes is gradually increased while the distance between potential electrodes is increased only when the observed potential difference across P_1 and P_2 becomes quite low [27]. The electrodes $C_1P_1P_2C_2$ are placed on straight line with $C_1C_2 \geq 1/5P_1P_2$; the apparent resistivity for this array is given by [4]

$$\rho_a = \pi \frac{(C_1C_2)^2 - (P_1P_2)^2}{4P_1P_2}\left(\frac{\Delta V}{I}\right), \quad (3)$$

where ρ_a is the apparent resistivity in ohm-m, C_1C_2 is the current electrode spacing in m, P_1P_2 is the potential electrode spacing in m, ΔV is the measured potential difference in Volt, and I is the injected current in Ampere.

Direct current (DC) resistivity sounding measurements using an ABEM Terrameter (model SAS 1000) electrical resistivity meter were collected at 272 stations. SAS stands for Signal Averaging System, a method whereby continuous reading is taken automatically and the results are averaged continuously. SAS results are more reliable than those using single shot system. The SAS 1000 permits natural or induced signals to be measured at extremely low levels, with excellent penetration and low power consumption [28]. Schlumberger electrode configuration arrays with a maximum current electrode separation (C_1C_2) ranging between 1000 and 2000 m were used. These spacings were adequate to ensure exploration depth to the groundwater target. The VES stations were distributed along a regular N-S grid of 500 m × 500 m.

At every VES station, current electrodes were spread out step by step. Apparent resistivity data were calculated and manually plotted in the field for checking the data quality. If distortions or errors appeared in data, measurements were repeated or the current electrode locations were changed to improve data quality. The author of this paper conducted the quality control of the field measurements and wrote the final technical report [29].

The VES data were plotted on a log-log graph with the electrode separation ($C_1C_2/2$ or AB/2) on the abscissa and the apparent resistivity (ρ_a) values on the ordinate. The advantages of using a log-log plot are that it emphasizes near surface resistivity variations and suppresses variations at greater depths, simply because interpretation of the results depends largely on the small variations in resistivity occurring at shallow depths [15].

Step-by-step matching using two layer curves and auxiliary curves was the main interpretation method until about 1980. Computer-based interactive modelling is now possible, even in field camps, and gives more reliable results, but the step-by-step approach is still often used to suggest initial computer models [30].

The resistivity soundings were inverted using the IPI2Win software. This software performs an automated approximation of the initial resistivity model using the observed data. This package uses a linear filtering approach for the forward modelling and the inversion is achieved by a regularized optimization based on Tikhonov's approach [31]. It works on an iterative mode by calculating at the end of each step: (a) an updated model of layer thickness and resistivity and (b) the misfit function between observed and calculated data. The starting model used during the inversion for each VES consisted of four to six layers and layering thickness was constrained using the calibrating nearby boreholes.

4. Results and Discussion

4.1. Aeromagnetic Data Interpretation. The TMI map of the study area is illustrated in Figure 6(b). Within the Maghnia region, the magnetic anomaly signature can be divided into two contrasting areas, that is, the north and the south. The TMI map offers a complex image with a very disturbed field throughout the northern part of the study area because of the relatively low 150 m altitude of the survey and of the many outcrops of volcanic rocks in the Traras Mountains. To the south, there is a broad long wavelength anomaly. It is a large asymmetric anomaly composed of a high in the south and a minimum pointing to the north. The positive component of the anomaly in the south is more intense to the east part than that to the west. This large anomaly trends in northeast-southwest direction and extends far to the west into the Moroccan territory. The large dimensions of the anomaly indicate a deep-seated origin.

Given that the anomaly has both positive and negative parts, it is likely induced by the present day Earth's magnetic field. Since the Eocene, the Earth's magnetic field in the study area had a direction within about 10° of the present one [32]. Probably, the deep intrusive body causing this anomaly is of Miocene age and belongs to postcollisional Neogene magmatism as most of the scattered volcanic rocks along the Mediterranean Maghreb Margin [33]. The reduced-to-pole magnetic map (Figure 6(c)) shows a shift of the anomalies to the north which shows that the reduction to pole transformation is done correctly. The study area is characterized by a positive anomaly and is surrounded on its northern and southern sides by large negative anomalies. Consequently, the magnetic basement in the study area is shallow relative to the adjacent areas. The uplift of the magnetic basement has induced faulting which is found in the surface geology (Figures 2 and 4). It is likely also that the uplift of the intrusion triggered faulting and fracturing in the underlying sedimentary strata.

One goal of our magnetic analysis was to locate any Quaternary basaltic flows which are groundwater bearing as is the case at Oujda (Morocco) and close to Maghnia city. However, there are no significant near surface magnetic anomalies in the VES survey area and so, we can conclude that there are no Quaternary basaltic flows at depth under the study area.

Figure 6(d) shows the map of the multiscale edge detection "worms" in part of the Maghnia plain. Most of the "worms" show that the majority of the identified contacts in the south of the study area have a northeast-southwest trend direction, and they highlight hidden deep faults that have the same direction as the known mapped faults. These hidden faults occur near recharge zones close to the mountains and they may identify locations for possible productive groundwater aquifers. The circular near surface "worms" in the northern part of the study area near the Traras Mountains delimit volcanic rock outcrops (Figures 6(a) and 6(d)).

The radially averaged power spectrum of the study area is characterized by three segments (Figure 7) with decreasing slopes relative to the wavenumber that give average depth estimates to the causative magnetic sources. The deepest sources have a depth of about 3840 m and probably correspond to either a hidden intrusive body or to the uplifted magnetic basement in the southern part of the study area. The intermediate sources have an average depth of 1630 m and probably correlate with volcanic strata in the northern part of the study area. These magnetic source depth estimates show that the magnetic basement in the study area is relatively shallow.

It is possible that some geothermal potential exists in the study area, because there has been recent volcanic activity in the Traras Mountains and Oujda area in Morocco and recent uplift of the magnetic basement as confirmed by this study. The northeastern Morocco in vicinity of Oujda and Berkane are a promising geothermal province. Here, geothermal water with a thermal gradient ranging between 29 and 90°C/Km is hosted mainly in the Liasic sedimentary reservoir [34].

4.2. Analysis and Interpretation of VES Data

4.2.1. Correlation to Existing Well Lithologies. Although 2D and 3D resistivity models are preferred for mapping the buried geology, a 1D resistivity model can give satisfactory results for a basic regional sedimentary geologic structure [35]. To validate our VES interpretation for the study area, three soundings were executed near wells with known lithology. The wells (Akid Lotfi, El Miad, and F15) are located in the north and northwest of the study area, very close to the Moroccan border. Figures 8(a), 8(b), and 8(c) show the 1D interpretation results and the correlation to the corresponding subsurface lithology.

The total depth of the Akid Lotfi well is 174 m (Figure 8(a)). The VES measured close to this borehole indicates the following: (1) it indicates a near surface dry layer with 9 m thickness that is made up of thin horizons of resistivity of 231, 63, and 6 ohm-m; (2) then it also indicates a medium to coarse gravel layer with a thickness of 86 m and a resistivity of 34 ohm-m, that is, the main aquifer; (3) the third clay and sand layer is characterized by an average resistivity of 3 ohm-m and a thickness of 19 m; (4) the fourth polygenic gravels layer has a thickness of 55 m and resistivity of 26 ohm-m; (5) from a depth of 151 m to the bottom of the borehole are clays with resistivity of 9 ohm-m.

The El Miad well has a depth of 150 m and a yield of 12 l/s (Figure 8(b)). A model with five geoelectric layers correlates with the lithology of this borehole. The geoelectric section is made up of (1) a 10 m thick layer having a resistivity of 10 ohm-m that corresponds to clays; (2) a 5 m thick second layer with a resistivity of 27 ohm-m that probably corresponds to clay with a small percentage of gravel; (3) a 41 m thick geoelectric layer with an average resistivity of 12 ohm-m that corresponds to gravels and clays; (4) an 80 m thick fourth layer with a resistivity 41 ohm-m that corresponds to coarse gravels with clay matrix; and (5) the lowermost layer that has a resistivity of 8 ohm-m and corresponds to clays. The third and fourth layers are the principle aquifers of this well.

The well F15 (Figure 8(c)) has a depth of 97 m. The interpretation of the VES sounding curve realized close to the borehole indicates that the geoelectric section is composed

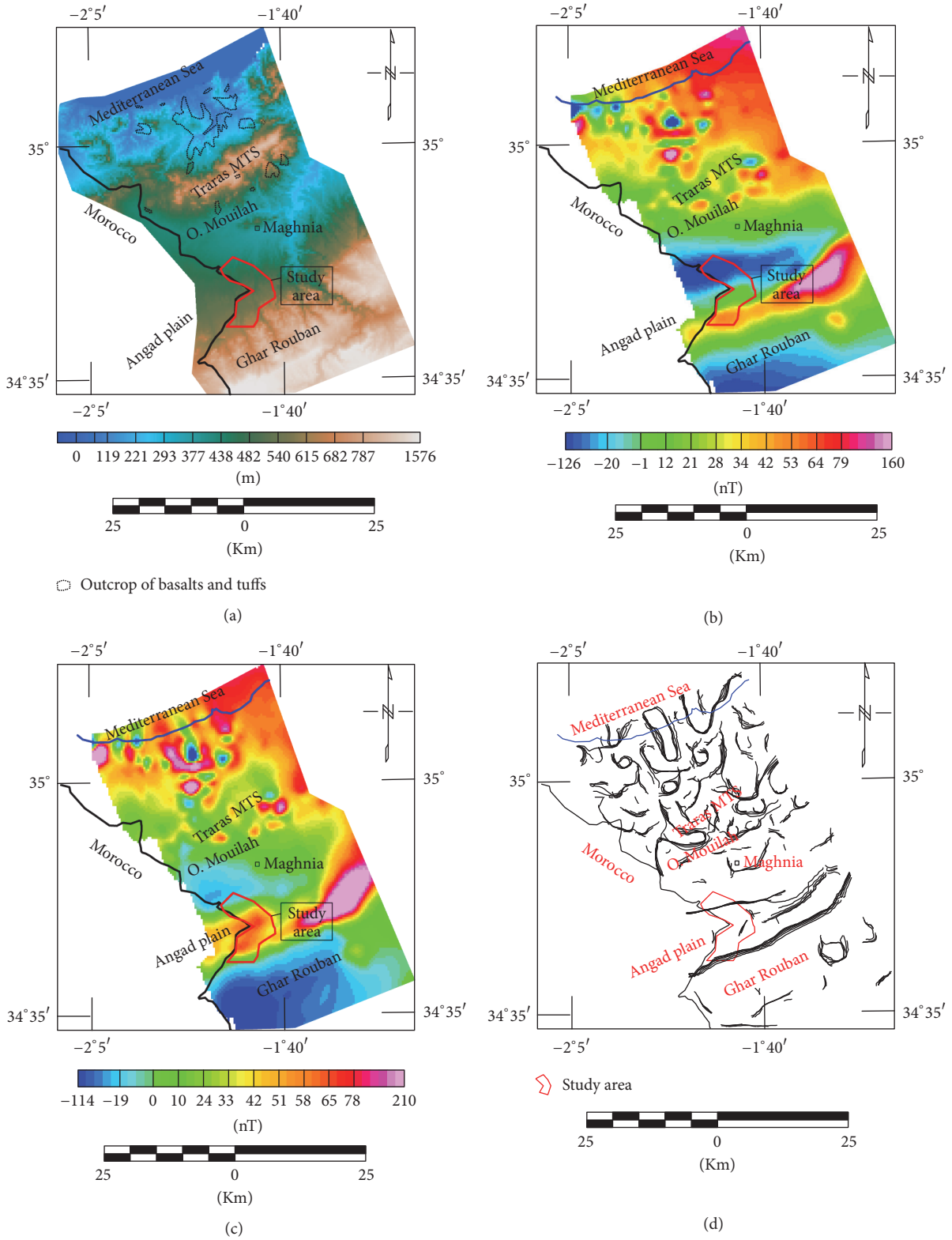

Figure 6: (a) Digital Elevation Model of the study area (SRTM data); (b) Total Magnetic Intensity (TMI) map for the study area; (c) reduced-to-the-pole TMI map for the study area and (d) map of the multiscale edge detection "worms" found in the study area.

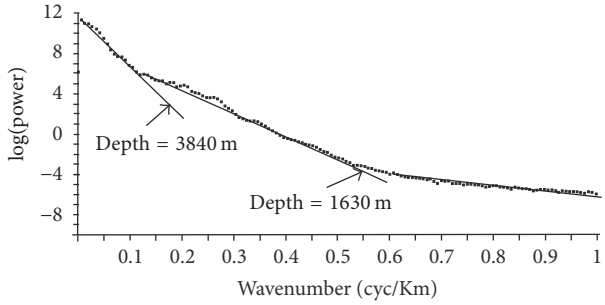

Figure 7: Radially averaged power spectrum of the study area.

Table 1: Interval resistivity variations of lithological units of the study area.

N	Formation	Age	Resistivity (ohm-m)	Thickness (m)
1	Clays	Plio-Quaternary	1–10	20–120
2	Resistive horizon (alluvium, gravel)	Plio-Quaternary	15–231	
	Aquifer		15–70	
3	Conductive horizon (marls)	Miocene	1–35	50–800
4	Sandstone	Miocene	150-150	
5	Sandstones	Jurassic (Oxfordian)	30–200	300–400
	Conductive horizon	Jurassic (Oxfordian)	1–83	

of six layers: (1) the first three thin near surface layers have high resistivities ranging from 58 to 372 ohm-m and a total thickness of 7.5 m that correspond to top soil and dry alluviums; (2) the 42 m thick fourth layer has an intermediate resistivity of 19 ohm-m and is composed of alluvium; (3) the fifth layer has a relatively high resistivity of 47 ohm-m and also is an aquifer; and (4) the sixth and bottom layer is the conductive geoelectric basement with an average resistivity of 12 ohm-m that is composed mainly of clays. The thin impermeable clay layers of this well are not well resolved by VES measurements but they probably divide the Plio-Quaternary into multiaquifer horizons.

Figure 8(d) illustrates a typical VES curve from the central part of the study area and the corresponding interpretation made to obtain estimates of the geoelectric layer parameters. The curve reflects the high-resistivity basement by the steeply rising apparent resistivities at large electrode spacings that correlates with the Oxfordian sandstones. VES curves for the Plio-Quaternary decline to very low resistivities at large electrode spacings (Figure 8(c)) that corresponds to Miocene marls, which form the substratum of the Plio-Quaternary aquifer.

Table 1 shows the correlation between the resistivity values and the different lithologies of the study area.

Figure 8(e) shows the distribution of aquifer thickness under the Maghnia plain established from drilling data [11]. The maximum thickness of Plio-Quaternary aquifer (90 m–130 m) is located in the northwest of the plain, an average thickness (50 m–90 m) occupies the central part of the plain along the Mehaguene, El Aounia, and El Abbes oueds, and a minimal thickness occurs close to Maghnia where it is ≤50 m.

4.2.2. Resistivity Maps. Figure 9 shows the apparent resistivity maps obtained for the electrode spacing AB of 100, 500, and 1000 m that are presented as vertical slices. According to these map slices, the study area displays roughly the same features in the vertical direction with the increasing depth of investigation. The study area can be divided into three zones that are noted in the lower slice of AB = 1000 m (I, II, and III). The first zone shows relatively higher resistivity values that correlate with Jurassic strata outcrop and the second zone is characterized by low resistivity values whereas the third zone shows moderate resistivities that correlate with Plio-Quaternary alluvium.

Figure 10 shows the apparent resistivity map for a spacing of AB = 500 m superposed on the surface geology map of Figure 2. The resistivity for this spacing varies from 10 ohm-m to 114 ohm-m. This map is very useful for distinguishing the lithologic layers at depths of about 100 m. In the central part of the study area we can see a northward deepening of the Oxfordian formations and a thickening of the Plio-Quaternary and Miocene infill with the steep resistivity gradients likely representing faults F1 and F3. The map also indicates that the conductive areas are clay-rich. The resistive area in the south of the study area correlates with the outcrop of Upper Jurassic formations, whereas it reflects a gravel-rich lithology in the northwest. The resistive strips in the north and northwest close to line 8 correspond to El Abbes and El Aounia oued channels. These 30–40 ohm-m resistive strips may correspond to buried channels and are probably favourable for groundwater accumulation.

4.2.3. Resistivity Cross Sections. Combining the interpretation of the VES curves with the geology of the area provides

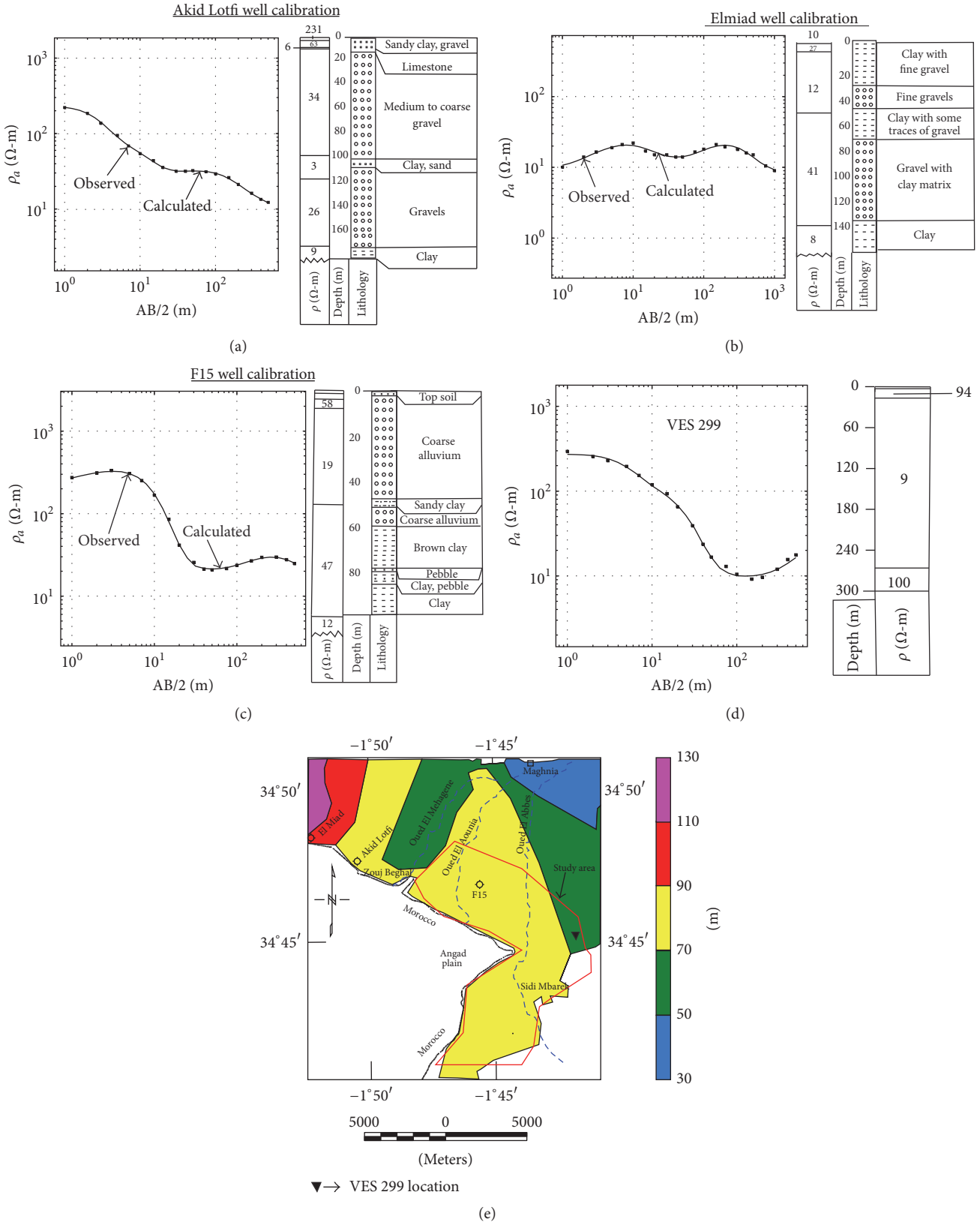

FIGURE 8: (a) VES calibration of the Akid Lotfi borehole; (b) VES calibration of the El Miad borehole; (c) VES calibration of the F15 borehole; (d) example of a VES field curve interpretation; and (e) thickness of the Plio-Quaternary aquifer.

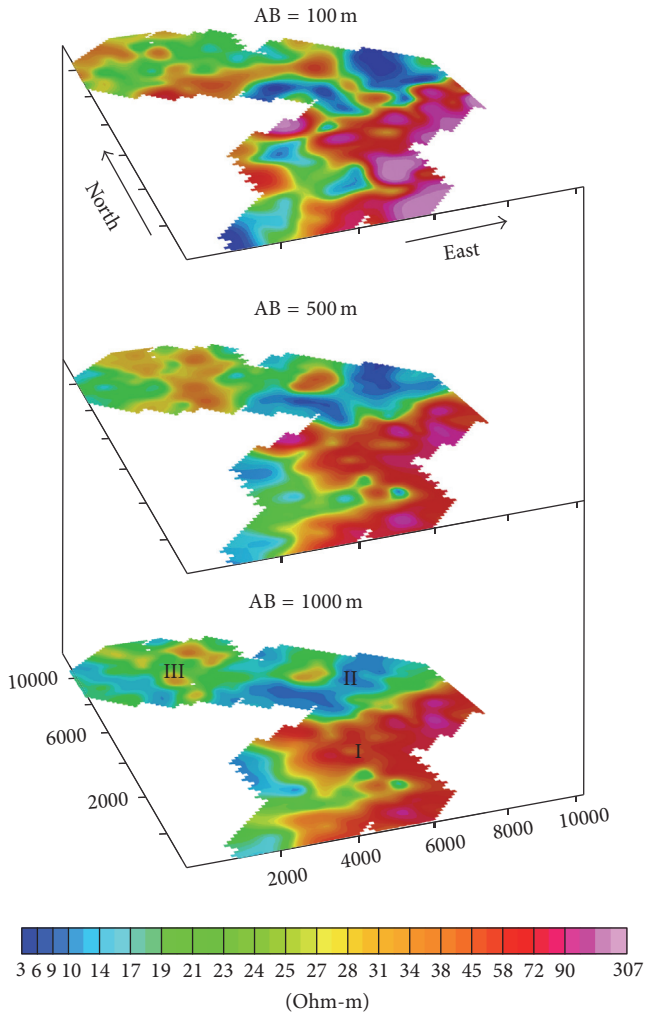

Figure 9: Apparent resistivity maps for the current spacings AB = 100 m; AB = 500 m; and AB = 1000 m.

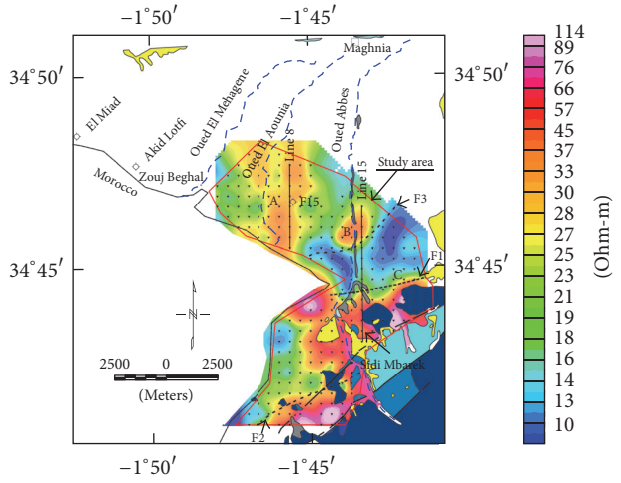

Figure 10: Apparent resistivity map for the current spacing AB = 500 m superposed on the geological map of the study area. Inverted triangles represent VES stations; heavy dashed lines represent interpreted faults. Heavy black lines correspond to the position of geoelectric sections.

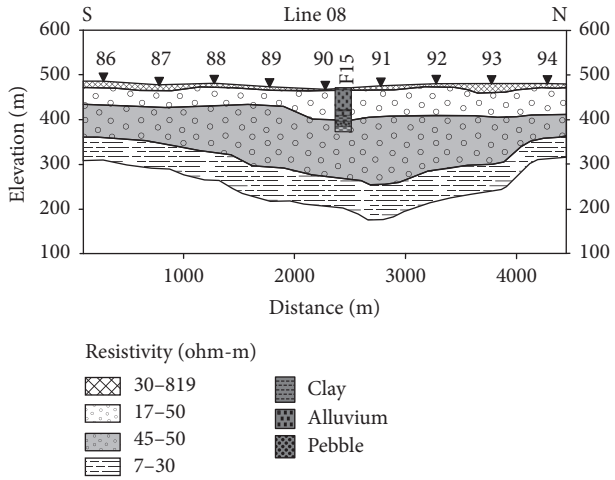

Figure 11: Geoelectric section for the line 08; for section position, see Figure 10.

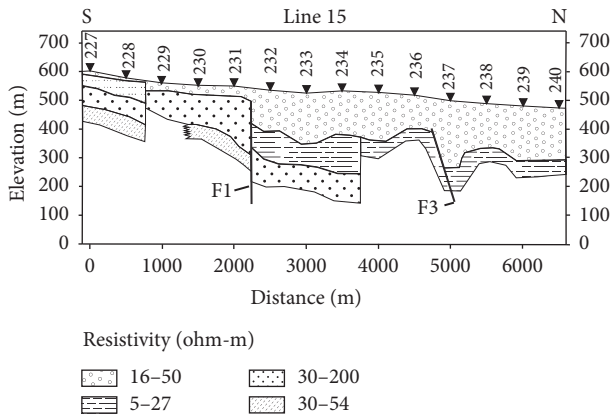

Figure 12: Geoelectric section for the line 15; for section position, see Figure 10.

two interpreted geoelectric sections along survey lines 8 and 15 (Figures 11 and 12).

Line 8 in the northern part of the study area is based on nine vertical electrical soundings from VES86 to VES94 with borehole F15 near its midpoint. Four geoelectric layers are distinguished in the resistivity section based on lithologic information from well 15 (Figure 11). The uppermost layer of dry topsoil has a large resistivity variation from 30 to 819 ohm-m with a thin thickness. It corresponds to the dry topsoil layer. The second layer shows resistivity values ranging from 17 to 50 ohm-m with a maximum thickness of 66 m under station VES91. This layer is probably composed of alluvium and indicates the probable existence of a groundwater potential. The third layer is relatively homogenous with an average resistivity of about 50 ohm-m and an average thickness of about 100 m. It is probably composed of Plio-Quaternary alluvium and may have a groundwater potential. The lowermost layer is characterized by low resistivity values of 7 to 30 ohm-m and composed of Plio-Quaternary clay or Miocene marls. The geoelectric section of this line shows quite good lateral continuity and coherence in resistivity and layer thickness.

Importantly, the average thickness along line 8 is of about 160 m, whereas previous studies, based on the shallow F15 well, gave an estimated maximum thickness of about 90 m. The extra layer thickness about doubles the aquifer's potential.

The second resistivity section (Figure 12) consists of 14 vertical electrical soundings and is calibrated against the known southern part of the Sidi Mbarek geologic section (Figure 4). The interpreted section is made up of four layers from stations VES227 to VES228, three layers from stations VES230 to VES234, and only two layers from stations VES235 to the end of the section. The top layer corresponds geologically to the Plio-Quaternary strata with high resistivities near surface and moderate resistivities at depth. The second layer correlates with the Miocene and has low resistivities. The third layer correlates with the Oxfordian sandstones with resistivity ranging between 50 and 120 ohm-m. To the south of F1 fault, the conductive substratum corresponds probably to the Callo-Oxfordian. To the north of the F1 fault, the Oxfordian sandstones undergo a northwards deepening; close to the F1 fault, they may constitute a good groundwater aquifer. Downdropped blocks from stations VES232 to VES234 toward the center of the plain confirm the pre-Miocene graben structure of the Maghnia plain. Normal NE-SW shallow (F1, F2, and F3) and deep faults highlighted by VES and magnetic data (Figures 6(d) and 10) occur near recharge zones situated close to bordering mountains. The highlighted faults give excellent conditions for the probable existence of productive groundwater aquifers. It is interesting to note that only the F2 fault corresponds to a known mapped one by the surface geology. The F1 and F3 faults highlighted by the present study are probably deep and hidden.

4.2.4. Proposed Groundwater Exploration Drill Sites. Zones A, B, and C (Figure 10) give an idea of the distribution of permeable strata in the study area. The moderate resistivity values of zones A and B indicate the presence of alluvium and gravel which are probably aquifer given that they are at depths which correlate with the water table (Figure 5). Also the section of line 8 presents a lithological succession similar to the calibrating wells (Figure 8), a near surface dry resistive layer, an intermediate layer with moderate resistivities (alluvium), and a conducting clayey substratum. This section gives a comprehensive hydrological information about the study area and its groundwater potential.

From the interpretation of the VES measurements and mapping of the Plio-Quaternary alluviums and Oxfordian sandstones that are recognized for their aquifer potentialities, three sites, indicated by A, B, and C (Figure 10), are proposed for drilling boreholes of 200 to 300 m depth:

(1) In the northwest zone around line 08, far from the well F15

(2) In the west of line 15 along El Abbes oued to check the Plio-Quaternary alluviums

(3) Close to fault F1 to test the potential for groundwater in the Oxfordian sandstones

5. Conclusion

This study demonstrates the important contribution of the resistivity and the aeromagnetic techniques as effective geophysical tools for exploring deep aquifers, a principal source of groundwater in the Maghnia plain of western Algeria.

The validity of the hydrogeological interpretation of the geophysical data is proved by several agreements between the resistivity distribution with depth and the aquifer characteristics. In particular, the most evident agreements are as follows:

(a) The moderate resistive layer aquifer (alluvium and gravel) and the water table are at the same depth.

(b) The interpreted geoelectric section and the calibrating wells show generally the same hydrogeological features.

The resistivity section of the Plio-Quaternary aquifer is mostly composed of four layers, characterized by an upper unsaturated layer of variable resistivities; a second layer with intermediate resistivities between 15 and 30 ohm-m with a maximum thickness of 66 m that is groundwater bearing; a third resistive saturated layer of 40 to 70 ohm-m with an average thickness of 100 m that is saturated; and a conductive layer of 1 to 10 ohm-m that appears to be composed of clays.

The interpreted resistivity map and two geoelectric sections illustrate the distribution of the different lithological units that underlie the study area within the graben structure. Faults interpreted from combination of aeromagnetic and VES data occur near recharge zones that are situated close to Upper Jurassic formations to provide excellent conditions for the probable existence of productive groundwater aquifers.

Relative resistive zones in the north and the northwest of the study area close to El Abbes and El Aounia oueds near lines 8 and 15 are the best targets for groundwater accumulation in the Plio-Quaternary aquifer. To check the groundwater potential of the Oxfordian sandstones, the central zone as close as possible to F1 fault is the best target for water well drilling to obtain maximum yield.

Competing Interests

The author declares that there is no conflict of interests regarding the publication of this paper.

Acknowledgments

The author is grateful to the Director of EURL BETA-Consults, Algiers, Algeria, for permitting the use and publication of the VES data.

References

[1] M. Boughriba, A.-E. Barkaoui, Y. Zarhloule, Z. Lahmer, B. El Houadi, and M. Verdoya, "Groundwater vulnerability and risk mapping of the Angad transboundary aquifer using DRASTIC index method in GIS environment," *Arabian Journal of Geosciences*, vol. 3, no. 2, pp. 207–220, 2010.

[2] Ministère des Ressources en Eau et de l'Environnement de la République Algérienne Démocratique et Populaire, http://www.mree.gov.dz.

[3] A. I. Ammar and S. E. Kruse, "Resistivity soundings and VLF profiles for siting groundwater wells in a fractured basement aquifer in the Arabian Shield, Saudi Arabia," *Journal of African Earth Sciences*, vol. 116, pp. 56–67, 2016.

[4] A. A. R. Zohdy, G. P. Eaton, and D. R. Mabey, "Application of surface geophysics to ground-water investigations," in *Techniques of Water-Resources Investigations of the U.S. Geological Survey, Book 2*, chapter 1, 1974.

[5] R. Kirsch, *Groundwater geophysics: a tool for hydrogeology*, Springer-Verlag, Berlin, Germany, 2006.

[6] V. J. S. Grauch, "Using high-resolution aeromagnetic surveys to map subsurface hydrogeology in sediment-filled basins: A Case Study Over The Rio Grande Rift, Central New Mexico, USA," *Exploration Geophysics*, vol. 32, no. 4, pp. 209–213, 2001.

[7] E. Chandrasekhar, S. L. Fontes, J. M. Flexor, M. Rajaram, and S. P. Anand, "Magnetotelluric and aeromagnetic investigations for assessment of groundwater resources in Parnaiba basin in Piaui State of North-East Brazil," *Journal of Applied Geophysics*, vol. 68, no. 2, pp. 269–281, 2009.

[8] P. M. Soupios, M. Kouli, F. Vallianatos, A. Vafidis, and G. Stavroulakis, "Estimation of aquifer hydraulic parameters from surficial geophysical methods: A Case Study of Keritis Basin in Chania (Crete—Greece)," *Journal of Hydrology*, vol. 338, no. 1-2, pp. 122–131, 2007.

[9] H. P. Patra, S. K. Adhikari, and S. Kunar, *Groundwater Prospecting and Management*, Springer Hydogeology, 2016.

[10] H. Djediai, M. Hadjel, K. Belaroui, and M. Benabdellah, "Study of water quality on the plain of Maghnia (Western Algeria)," *Desalination and Water Treatment*, vol. 52, no. 10-12, pp. 2039–2046, 2014.

[11] K. Baba Hamed, *Hydrodynamique et modélisation d'une nappe alluviale, validation par l'approche géostatistique. Application à la nappe de la plaine de Maghnia (NW Algérien) [Ph.D. thesis]*, University of Tlemcen, 2007.

[12] Office National de la Recherche Géologique et Minière (ORGM), "Geologic Map of Maghnia, scale 1: 50 000," map, 1995.

[13] A. Achachi, "Etude hydrogéologique des Monts de Tlemcen," Internal Report, ANRH, 1996.

[14] M. Bonnet, "Etude hydrogéologique de la plaine de Maghnia," Report S.E.S no.59/ GE. Oran, 1965.

[15] Agence Nationale des Ressources Hydriques (ANRH), "Résultats des pompages d'essai effectuées sur puits et forages de Maghnia- plaine des Angads," Direction Régionale Ouest, 1988.

[16] M. Ameur and F. Saad, "Etude hydrogéologique de la plaine de Maghnia," Mémoire d'Ingéniorat, Université d'Oran, 1990.

[17] K. Allek and M. Hamoudi, "Regional-scale aeromagnetic survey of the south-west of Algeria: a tool for area selection for diamond exploration," *Journal of African Earth Sciences*, vol. 50, no. 2-4, pp. 67–78, 2008.

[18] D. Boubaya, K. Allek, and M. Hamoudi, "Is there a hidden near surface salt diapir in the Guelma Basin, north-east of Algeria?" *Journal of Applied Geophysics*, vol. 73, no. 4, pp. 348–356, 2011.

[19] I. C. Briggs, "Machine contouring using minimum curvature," *Geophysics*, vol. 39, no. 1, pp. 39–48, 1974.

[20] Geosoft, *Oasis Montaj 7.01 Mapping and Processing System*, Geosoft, 2008.

[21] V. Baranov, "A new method for interpretation of aeromagnetic maps: pseudo-gravimetric anomalies," *Geophysics*, vol. 22, no. 2, pp. 359–382, 1957.

[22] N. Archibald, P. Gow, and F. Boschetti, "Multiscale edge analysis of potential field data," *Exploration Geophysics*, vol. 30, no. 2, pp. 38–44, 1999.

[23] P. Hornby, F. Boschetti, and F. G. Horowitz, "Analysis of potential field data in the wavelet domain," *Geophysical Journal International*, vol. 137, no. 1, pp. 175–196, 1999.

[24] I. M. A. Vos, F. P. Bierlein, M. A. Barlow, and P. G. Betts, "Resolving the nature and geometry of major fault systems from geophysical and structural analysis: the Palmerville Fault in NE Queensland, Australia," *Journal of Structural Geology*, vol. 28, no. 11, pp. 2097–2108, 2006.

[25] A. Spector and F. S. Grant, "Statistical models for interpreting aeromagnetic data," *Geophysics*, vol. 53, pp. 1587–1591, 1970.

[26] C. R. Fitts, *Goround Water Science*, Elsevier, 2nd edition, 2013.

[27] S. B. Singh, B. Veeraiah, R. L. Dhar, B. A. Prakash, and M. T. Rani, "Deep resistivity sounding studies for probing deep fresh aquifers in the coastal area of Orissa, India," *Hydrogeology Journal*, vol. 19, no. 2, pp. 355–366, 2011.

[28] ABEM, *Instruction Manual for the Terrameter SAS/4000 SAS/1000*, ABEM Instrument AB, 2010.

[29] EURL BETA-Consults, "Etude géophysique par la méthode de sondage électrique dans la région de Maghnia," Internal Report, 2012.

[30] J. Milsom and A. Eriksen, *Field Geophysics*, John Wiley & Sons, 4th edition, 2011.

[31] C. Bobachev, *IPI2Win: a windows software for an automatic interpretation of resistivity sounding data [Ph.D. thesis]*, Moscow State University, 2002.

[32] T. H. Torsvik, R. Van der Voo, U. Preeden et al., "Phanerozoic polar wander, palaeogeography and dynamics," *Earth-Science Reviews*, vol. 114, no. 3, pp. 325–368, 2012.

[33] R. C. Maury, S. Fourcade, C. Coulon et al., "Post-collisional Neogene magmatism of the Mediterranean Maghreb margin: a consequence of slab breakoff," *Comptes Rendus de l'Academie de Sciences*, vol. 331, no. 3, pp. 159–173, 2000.

[34] A. E. Barkaoui, Y. Zarhloule, M. Verdoya, V. Pasquale, and H. Lahrach, "Progress in understanding the geothermal sedimentary basins in northeastern Morocco," *Journal of African Earth Sciences*, vol. 97, pp. 1–8, 2014.

[35] A. Hördt, K. Strack, K. Vozoff, and P. A. Wolfgram, "Resolving resistive layers using joint inversion of LOTEM and MT data," in *Theory and Practice of Geophysical Data Inversion*, A. Vogel, A. K. M. Sarwar, R. Gorenflo, and O. I. Kounchev, Eds., pp. 147–158, Vieweg, Wiesbaden, Germany, 1992.